Profiling and Predicting Distinct Tau Progression Patterns: An Unsupervised Data-Driven Approach to Flortaucipir Positron Emission Tomography

Duygu Tosun[1,2,#], **Pamela Thropp**[2], **Sudeepti Southekal**[3], **Bruce Spottiswoode**[4], **Rachid Fahmi**[4] **Alzheimer's Disease Neuroimaging Initiative**[*]

[1]Department of Radiology and Biomedical Imaging, University of California San Francisco, San Francisco, CA, USA 94143

[2]Northern California Institute of Research and Education, San Francisco, CA, USA 94121

[3]Eli Lilly and Company, Philadelphia, PA, USA 19104

[4]Siemens Medical Solutions USA, Inc., Molecular Imaging, Knoxville, TN, USA 37932

Abstract

INTRODUCTION: How to detect patterns of greater tau burden and accumulation is still an open question.

METHODS: An unsupervised data-driven whole-brain pattern analysis of longitudinal tau-PET was used first to identify distinct tau accumulation profiles and then to build baseline models predictive of tau-accumulation type.

RESULTS: The data-driven analysis of longitudinal flortaucipir-PET from ADNI, AVID-05, and HABS studies (N=348 cognitively unimpaired, N=188 MCI, N=77 dementia), yielded three distinct flortaucipir-progression profiles: stable, moderate-accumulator, and fast-accumulator. Baseline flortaucipir levels, Aβ-positivity, and clinical variables, identified moderate- and fast-accumulators with 81% and 95% positive predictive values, respectively. Screening for fast tau accumulation and Aβ-positivity in early-AD, compared to Aβ-positivity with variable tau progression profiles, required 46%-77% less sample size to achieve 80% power for 30% slowing of clinical decline.

DISCUSSION: Predicting tau progression with baseline imaging and clinical markers could allow screening of high-risk individuals most likely to benefit from a specific treatment regimen.

Keywords

Alzheimer's disease; tau pathology; disease pathology progression; sample size

BACKGROUND

Alzheimer's disease (AD) is an irreversible and progressive neurodegenerative disease[1]. AD is characterized by the presence of aggregated amyloid-β (Aβ) plaques and by tau-containing neurofibrillary tangles, leading to neurodegeneration, and then to cognitive and clinical decline[2]. Various Aβ-targeting therapies are being developed, with the expectation that Aβ reduction would slow both tau accumulation and cognitive decline. Thus far, treatments have been largely ineffective in slowing cognitive decline, with modest beneficial clinical effects being reported only recently[3-6]. Data from recent clinical trials and observational cohorts, provide supportive evidence that Aβ is a key driver of tau[7]. Moreover, Aβ and tau together have been shown to promote cognitive decline[8-11]. Although Aβ accumulation is strongly associated with AD, disease severity and progression have been more closely linked to tau. Several longitudinal studies have investigated the spread of tau in AD and have suggested that the density and spatial distribution of tau may have implications both for the future tau spread and cognitive decline across the AD clinical spectrum[8, 9, 11].

A recent Aβ-lowering therapy trial used baseline tau levels, measured with positron emission tomography (PET), to recruit participants and used the change in tau-PET burden as a secondary outcome[5]. In that trial, participants with the lowest baseline tau-PET burden showed greater clinical benefit with better primary and secondary cognitive and functional scores in a post hoc analysis, suggesting that Aβ-lowering therapies result in greater clinical outcomes in patients in whom tau is not yet widespread, and that early tau may represent an important treatment window where intervention is more likely to have a positive outcome if delivered to individuals on an aggressive trajectory of AD protein accumulation and in temporal proximity to rapid AD protein burden acceleration.

In this quest to identify patients who will most likely benefit from a specific treatment based on their risk for greater tau accumulation, the question of how to detect patterns of greater tau-burden and accumulation is largely unanswered. The disease course and the potential to successfully target the pathology varies greatly among individuals[12], and heterogeneity in tau accumulation and spread patterns is likely a contributing factor. Using cross-sectional tau-PET images and a data-driven approach, researchers have identified four distinct trajectories of tau in AD[13], and have made longitudinal inferences about the natural history of tau progression. Such methods aiming at identifying distinct spatiotemporal trajectories of tau accumulation from a single imaging time-point do not often exploit tau progression information over time, when available, which might be more important for an accurate identification of tau spatiotemporal trajectories.

With the growing collection of longitudinal tau-PET, many studies show intercorrelation among regions representing stages of tau accumulation over time, which greatly depends on tau-burden at baseline[9, 14-16]. Machine learning-based approaches have been proposed to predict individualized rates of future tau accumulation and to identify populations at greatest risk of future tau accumulation[17], which might have great translational impacts on clinical trials. However, in majority of published studies, the magnitude of accumulation rates is usually based on change at last available measurements reflecting the patient's current status, without accounting for potential heterogeneity in dynamics of temporal profiles and in spatial patterns. Thus, there is a need to evaluate the distinct patterns of tau accumulation using a method that jointly exploits the whole history of longitudinal measurements of all considered spatial tau sites to design optimal tau inclusion criteria for clinical trials.

This work aimed to determine distinct AD tau accumulation profiles among elderly subjects in three large longitudinal cohorts of cognitively unimpaired (CU) individuals, individuals with mild cognitive impairment (MCI), and individuals with a clinical AD dementia diagnosis. Different from previous studies, we propose an unsupervised, data-driven, whole-brain, longitudinal pattern analysis approach leveraging the spatially and temporally rich information provided by longitudinal tau-PET. We first identified distinct subtypes of tau accumulation profiles from longitudinal observational data and then built baseline models predictive of these tau accumulation profiles.

METHODS

Participants

Data were obtained from a total of N=613 individuals from three independent observational cohorts: the Alzheimer's Disease Neuroimaging Initiative (ADNI) [18], a phase 2/3 study undertaken as part of Avid Radiopharmaceuticals' clinical development program for their flortaucipir F-18 PET radiotracer (AVID-05) [9], and Harvard Aging Brain Study (HABS) [19]. ADNI data used in the preparation of this article were obtained from the ADNI database (adni.loni.usc.edu). The ADNI was launched in 2003 as a public-private partnership, led by Principal Investigator Michael W. Weiner, MD. The primary goal of ADNI has been to test whether serial magnetic resonance imaging (MRI), positron emission tomography (PET), other biological markers, and clinical and neuropsychological assessment can be combined to measure the progression of mild cognitive impairment (MCI) and early Alzheimer's disease (AD). For up-to-date information, see www.adni-info.org.

The population in this study included participants with an Aβ PET scan using either ^{18}F-florbetapir (ADNI and AVID-05) or ^{11}C-PIB (HABS) and two or three ^{18}F-flortaucipir tau PET scans within three years of study participation. Aβ PET scans were previously processed using published cohort-specific processing streams, and Aβ-positivity was defined using previously established thresholds: standardized uptake value ratio (SUVR) = 1.1021 for ^{18}F-florbetapir PET (ADNI and AVID-05) [20] and distribution volume ratio (DVR) = 1.20 for ^{11}C-PIB PET (HABS) [21]. Based on these thresholds, for each subject, we utilized the Aβ +/− status, instead of the actual composite SUVR value, as one of the prediction parameters, and hence, no harmonization of our multi-site Aβ PET data was required.

Tau PET imaging

Flortaucipir PET data acquisition procedures for each cohort have been described previously [22-24]. To minimize the impact of inter-scanner variabilities as well as that of differences in acquisition and reconstruction protocols, flortaucipir PET scans from all three cohorts were smoothed to an intrinsic smoothness of 8mm full-width-half-max. Subsequently, the data underwent preprocessing using the same pipeline recommended by ADNI PET Core (https://adni.loni.usc.edu/). Motion corrected, averaged, and smoothed flortaucipir images were each rigidly co-registered to its respective native T1-weighted MRI, intensity normalized using an eroded subcortical white matter mask to estimate tau SUVR images [24, 25], and corrected for partial-volume-effect using an T1 MRI-based approach [26]. Each T1-weighted anatomical MRI was segmented into cortical, subcortical, cerebellar, and white matter regions-of-interest (ROIs) using the automated open-source processing framework, Advanced Normalization Tools (ANTs), by first applying a bias field correction followed by a deformable registration to warp a template to the subject brain image, and then using a multivariate MRF-based segmentation method to perform segmentation [27]. The entire cortex of each subject's brain was then parcellated into 35 bilateral ROIs based on a previously published volumetric Desikan-Killiany-Tourville atlas [28].

Previous studies on the progression of tau accumulation focused on algorithmic rate estimates either from *a priori* selected anatomical parcellations (e.g., medial temporal lobe or inferior temporal gyrus) or target volumes of interest consisting of a weighted average of voxels or meta-regions of interest found to contribute to discrimination between clinical groups (e.g., Aβ-positive CU *vs.* Aβ-negative CU or Aβ-positive cognitively impaired (CI) *vs.* Aβ-positive CU) [9, 15]. Findings in both neuropathology studies and emerging data with tau PET tracers support the view for the predominance of stereotypical tau PET patterns in individuals across the AD spectrum [29]. Leveraging the knowledge of the stereotypical patterns of tau accumulation brain sites and aiming for a granular regional quantification of tau pathology, we defined tau accumulation sites of interest bilaterally following the six-stage operationalized neuropathologic staging scheme proposed by Braak *et al.* [30]. Furthermore, previous studies showed that a lateralized difference in Braak tau stages might be present in AD [31, 32]. Therefore, we analyzed ten Braak tau composite ROIs from left and right hemispheres: Left/Right Braak-I (entorhinal cortex), Left/Right Braak-III (amygdala, parahippocampal, fusiform, and lingual gyri), Left/Right Braak-IV (middle temporal, caudal anterior cingulate, rostral anterior cingulate, posterior cingulate, isthmus cingulate, inferior temporal, insula, and temporal pole), Left/Right Braak-V (superior frontal, lateral orbitofrontal, medial orbitofrontal, frontal pole, caudal middle frontal, rostral middle frontal, pars opercularis, pars orbitalis, pars triangularis, lateral occipital, supramarginal, inferior parietal, superior temporal, superior parietal, precuneus, banks of superior temporal sulcus, and transverse temporal cortex), and Left/Right Braak-VI (pericalcarine, postcentral, cuneus, precentral, and paracentral cortices). Braak-II (hippocampus) was excluded due to flortaucipir signal spill-in from the choroid plexus. Regional flortaucipir SUVR values were corrected for normal confounding effects of age and sex observed in Aβ-negative CU individuals.

We recognize that MRI-based pre-processing of tau-PET scans may not be feasible or widely available due to various reasons, such as lack of access to MRI scans or contraindications for MRI in some patients. In order to evaluate the robustness of the tau progression prediction method, described below, to different tau-PET processing frameworks, we additionally computed and utilized regional SUVR values from ADNI participants using a PET-only processing pipeline without correction for partial volume effects [33]. The corresponding results are included in the supplementary material (Figure S1).

Statistical analysis

To identify distinct clusters of longitudinal tau progression profiles, we allowed all individual regional flortaucipir measures from all time points to factor into an unsupervised Bayesian multivariate clustering of the longitudinal data using a mixture of multivariate generalized linear mixed (MMGLM) model. We chose to use an unsupervised clustering approach in order to discover distinct patterns of longitudinal tau accumulation without imposing any prior assumptions on region selection nor on outcome associations. This approach allowed us to explore the data without being influenced by previously identified tau accumulation results and to identify novel patterns that may not have been apparent using traditional supervised approaches. The MMGLM model uses a random-effect structure when estimating heterogeneity between individuals' longitudinal progression curves, allowing estimates of distinct clusters of accumulators and probabilities of cluster membership. Specifically, a model was built whereby all regional flortaucipir SUVR values from all time points were included as multivariate outcome variables (i.e., multivariate longitudinal feature space) and regressed on time in the study while accounting for inter-regional dependence and irregular time sampling. A random intercept and slope for each subject were included in the model to adjust for multiple measurements over time and for baseline variability across participants. This clustering approach is a K-means-style procedure in that the number of clusters must be chosen *a priori*. Therefore, the optimum number of clusters with distinct tau progression patterns was estimated based on deviance statistics calculated by using multiple numbers of clusters ranging from one to five.

We assessed the differences among the estimated tau progression clusters based on the baseline demographic, clinical, and biomarker variables of interest, including age, sex, years of education, ethnicity, race, *APOE*-ε4 genotype, Aβ-positivity, regional tau burden, AD meta-ROI atrophy [34], cerebrovascular white matter lesion (WML) burden, the Mini-Mental State Examination (MMSE), Clinical Dementia Rating – Sum of Boxes (CDR-SB), the Alzheimer's Disease Assessment Scale-Cognitive Subscale (ADAS-Cog), MCI diagnosis, dementia diagnosis, and psychiatry symptoms (Geriatric Depression Scale or GDS), using Wilcoxon rank-sum test and Fisher's exact test for continuous and categorical variables, respectively. Where repeated measures were available for the variables of interest, we also calculated the differences between clusters based on the longitudinal change in these variables using mixed effect regression assuming an independent correlation structure and conditional on a random intercept.

We then tested the ability to predict, for each subject, the tau progression cluster membership from a set of candidate baseline variables using multiclass random-forest classification (MC-RFC) modeling. Candidate predictors for MC-RFC modeling were limited to factors available for all three study cohorts: age, sex, years of education, *APOE* ε4 genotype, Aβ-positivity, regional flortaucipir SUVR, and MMSE, which are also commonly collected in clinical trials. Random 60% and 40% split was used to train and test the MC-RFC model. The choice of the 60-40 split was based on the size of our dataset and to ensure an adequate number of samples in both the training and testing sets. To ensure the stability of the results, we repeated the random train-test split 100 times to evaluate the performance of our model with different splits.

To assess the value of the estimated flortaucipir-progression profiles, we estimated sample sizes required for various clinical trial enrichment scenarios to achieve 80% power to detect a range of assumed treatment effect sizes (20-50%) for 18-month trials for Aβ+ early AD, AD, and MCI populations, and 48-month trials for Aβ+ CU with cognitive outcome assessment performed every six months, using longitudinal clinical measures from ADNI participants. Cognitive outcome measures of interest included changed in ADAS-Cog13, CDR-SB, and Preclinical Alzheimer Cognitive Composite (PACC) as these are the tools typically used in AD clinical trials [35]. Change in flortaucipir SUVR in the temporal metaROI comprising the bilateral entorhinal cortex, amygdala, fusiform gyrus, and inferior and middle temporal cortices [36] was also considered as an outcome measure of interest as this measure has been included in the recent AD trials as a secondary outcome measure. The enrichment scenarios considered demographic and clinical inclusion criteria used in the current design of clinical trials together with (1) screening for Aβ biomarker evidence only; and (2) screening for both baseline Aβ biomarker evidence and for flortaucipir-progression profiles. Sample size calculations informed by ADNI data were performed assuming a linear mixed-effects model analysis using standard methods described elsewhere [37].

All analyses were performed using R software, v4.1.2 (www.r-project.org). Unsupervised MMGLM clustering model, MC-RFC predictive modeling, and sample size calculations were performed using the following R packages, *MixAK*, *mlr*, and *longpower*, respectively.

RESULTS

Participants characteristics

Both ADNI (as of Sept 2022) and AVID-05 datasets contained CU and demented participants, whereas HABS (date release 2.0; July 2021) dataset was composed of CU participants only. Included participants were all 50 years or older. This resulted in 1,515 data points from 613 participants with characteristics shown in Table 1 and Table S1.

Distinct Flortaucipir Progression Groups

The MMGLM clustering model resulted in three distinct flortaucipir progression groups (Figure 1). Based on the longitudinal flortaucipir progression profiles, these three distinct groups are herein referred to as 1) "stable" group presenting with minimal flortaucipir-accumulation (mean SUVR of 0.011–0.019 SUVR units/year) across all Braak regions;

2) "moderate accumulator" group with slow flortaucipir-accumulation rates (0.030–0.051 SUVR units/year) predominantly in Braak III–V regions; and 3) "fast-accumulator" group with accelerated flortaucipir-accumulation rates (0.034–0.11 SUVR units/year) in the Braak III–VI regions.

Stratification of participants into the three flortaucipir progression clusters results in 440 participants assigned to the stable group, 96 participants to the moderate flortaucipir-accumulator group, and 38 participants to the fast accumulator group. The remaining 39 participants out of 613 (6%) had uncertain classification based on highest posterior density credible intervals (Table 2).

Leave-dataset-out analyses replicated the optimal three-group solution, with the percentage overlap for participants assigned to the same cluster ranging from 86.26% to 94.86%, with an average overlap of 92.70%.

Characteristics of the three flortaucipir progression groups are reported in Table 2 and Figure 2. The groups did not differ statistically in ethnoracial and sex distributions. The fast accumulators compared to stable and moderate accumulator groups had on average one year less years of education, which was statistically significant. Ninety-eight percent of Aβ-negative CU individuals presented with stable flortaucipir-progression, and 68% of the Aβ-positive individuals with CI and dementia presented with moderate or fast flortaucipir-progression profiles. The prevalence of moderate and fast flortaucipir-progression profiles increased with Aβ-positivity, cognitive impairment, and *APOE-ε4* carrier status.

The distribution of cases with two *vs.* three timepoints of flortaucipir PET scans was similar among all three groups. However, moderate accumulator and fast accumulator groups had on average of 0.5 years and 0.7 years shorter duration of flortaucipir PET follow-ups, respectively, reflecting study design differences across ADNI, AVID-05, and HABS.

At the time of the first flortaucipir PET observation, moderate accumulators – in comparison to their stable counterparts – were characterized by older age, higher prevalence of *APOE ε4* carriers, greater WML burden, higher prevalence of Aβ+, greater flortaucipir burden, thinner cortex in the AD meta-ROI, worse global cognitive performance in MMSE and ADAS-Cog, worse clinical symptoms (CDR-SB), and higher prevalence of clinical MCI diagnosis (Table 2 and Figures 2-3). Moderate accumulators had greater rates of cognitive and clinical decline overall (MMSE, ADAS-Cog, CDR-SB). In addition, they acquired more depressive symptoms (GDS) over time compared to those within the stable flortaucipir progression group.

Similarly, fast accumulators, compared to their stable and moderate accumulator counterparts, were characterized by greater flortaucipir burden, worse global cognitive performance in MMSE and ADAS-Cog, and worse clinical symptoms (CDR-SB). However, they were younger with higher prevalence of clinical dementia diagnosis at the time of first flortaucipir PET scan (Table 2 and Figures 2-3). Fast accumulators also had a higher prevalence of *APOE ε4* carriers, Aβ+ status, and thinner cortex in the AD meta-ROI compared to the stable group but did not differ in these variables compared to the moderate

accumulators. Finally, fast accumulators had greater cognitive and clinical decline (MMSE, ADAS-Cog, CDR-SB) over time compared to the stable and moderate accumulator groups.

Predicting flortaucipir progression groups

Next, we tested to what extent the flortaucipir progression groups could be predicted using an MC-RFC model based on the baseline variables of interest. This is an imbalanced classification problem because of the skewed class distribution towards the stable group, making it harder to build a predictive model for moderate accumulator and fast accumulator groups. Further, while most classifiers assume that misclassification costs are the same for false negative and false positive predictions, the cost of false positive predictions may be conceptually greater than the cost of false negative predictions, or vice versa, in clinical practice and in clinical trial settings. The classification problem was then set to minimize the total misclassification cost instead of optimizing the overall accuracy using a cost-sensitive learning scheme to address these challenges. Imbalanced classification costs were assigned based on the inverse class distribution.

Results show that baseline flortaucipir uptake in bilateral Braak-IV, Braak-III, Braak-V, and Braak-I ROIs, Aβ positivity status, and MMSE ranked with high variable importance in predicting the longitudinal flortaucipir progression group (Figure 4), while sex, age, *APOE ε4* carrier status, and baseline flortaucipir uptake in bilateral Braak-VI ROI were among the variables with low-ranking importance. The MC-RFC reached an overall accuracy of 92% (95% CI: [91%, 93%]) and balanced accuracy of 87% [86%, 89%] with a positive predictive value (PPV) of 81% [77%, 85%] for the moderate accumulators and 95% [92%, 100%] for the fast accumulators, and a negative predictive value (NPV) of 94% [93%, 95%] for the stable group.

Required Effect Size and Sample Size for Clinical Trials

The effectiveness of screening for evidence of Aβ pathology with variable tau progression was compared to joint screening for evidence of Aβ and tau accumulation profiles (stable, moderate accumulator, and fast accumulator), as depicted in Figure 5 and summarized in Table 3. Figure 5 shows the treatment effect sizes plotted against sample sizes for the four enrichment schemes in an 18-month placebo-controlled trial for early AD. The figure highlights the combinations required to achieve 80% power for clinical outcome measures of ADAS-Cog, CDR-SB, PACC, as well as biomarker outcome measures of tau burden in the temporal metaROI. Additionally, Table 3 summarizes the sample size requirements for Aβ+ MCI, Aβ+ AD, and Aβ+ CU populations for the same scenarios of tau accumulation profile-based enrichment. To achieve 80% power for a 30% slowing of clinical decline in ADAS-Cog13 compared with placebo in an 18-month trial for early AD, a sample size of N=97 of Aβ+ and fast tau accumulator participants per group was required. This is in contrast to N=212 of Aβ+ and moderate tau accumulator participants and N=266 of Aβ+ participants with variable flortaucipir progression profiles (i.e., no tau progression screening). We estimated a reduction in required sample size of 2.7-4.3-fold for clinical outcome measures of ADAS-Cog13, CDR-SB, and PACC, and a 1.8-fold reduction for change in temporal meta-ROI tau SUVR as the outcome measure in an 18-month trial for early AD, when comparing cohort selection based only on Aβ-positivity

with variable tau progression profile to selection based on both Aβ-positivity and fast tau accumulation profile predictions. Screening for fast, but not moderate, tau accumulation profile participants within Aβ+ AD yielded a 1.7-2.1-fold reduction in required sample size to detect 30% slowing of the clinical outcome measures of interest, while a 1.4-fold reduction in required sample size to detect 30% slowing of change in tau SUVR in temporal metaROI was observed only in the screening scenario for moderate tau accumulation. In contrast, screening for Aβ+ MCI participants with either moderate or fast tau accumulation profiles consistently yielded 1.2-12.3-fold reduction in required sample size to detect 30% slowing of both the clinical and temporal metaROI tau outcome measures of interest. Finally, when screened for moderate tau accumulation profiles, the sample size required in a 4-year placebo-controlled trial for Aβ+ CU was reduced by 4.5-6.8-fold to detect 30% slowing of both the clinical and temporal metaROI tau outcome measures of interest.

DISCUSSION

We identified three groups of flortaucipir progression profiles: stable, moderate-accumulator, and fast-accumulator. The data-driven clustering results represent an extension of prior findings on tau-accumulators. Specifically, 1) Aβ-positive, *APOE-ϵ4* carriers with MCI or dementia due to AD diagnosis are more likely to progressively accumulate tau, whereas Aβ-negative CUs tend to present with stable tau; 2) the faster the pace of tau accumulation, the greater the rate of cognitive decline and neurodegeneration; and 3) baseline tau levels together with Aβ-positivity and severity of clinical and cognitive symptoms predict a subsequent increase in tau levels. Longitudinal tau-PET studies consistently reported that tau progresses faster in individuals with Aβ[15, 38], albeit tau accumulation is seen in some brain regions among elderly without Aβ deposition[39]. These studies have similarly concluded that Aβ deposition is a prerequisite for tau spread to the cortex which coincides with onset of clinical symptoms[40, 41], baseline tau levels predict subsequent tau accumulation[16, 17], and both baseline and progressive accumulation of tau correlate with neurodegeneration and cognitive decline[8, 11, 16, 42]. In line with prior research, moderate-accumulators and fast-accumulators in our study presented with greater baseline tau levels, worse baseline cognitive performances and clinical diagnoses, and greater rates of clinical decline in a dose-dependent manner. Our results strengthen previous observations that cortical tau-burden increases particularly in people with significant Aβ pathology and that, in these people, the greater is tau-burden at baseline the more it accumulates over time.

We also observed additional clinical and biomarker characteristics unique to these tau-accumulator groups. Compared to their stable counterparts, moderate-accumulators were older with greater cerebrovascular WML-burden and more depressive symptoms' onset over time, whereas fast-accumulators were younger. Older age at symptom onset is associated with lower tau and Aβ[43], consistent with established evidence that a younger person is more likely to only have AD pathology (Aβ and tau) for any given level of cognitive impairment[44], and AD neuropathological changes are strongly associated with rapid disease progression in younger elderly[45]. One explanation for observed younger age in the fast-accumulators could be that individuals who had Aβ early had a more rapid Aβ accumulation leading to rapid aggregation of tau tangles. In contrast, an older person is more likely to have non-AD pathologies. For instance, lower levels

of Aβ-burden are often observed in dementia patients with cerebrovascular burden[46]. Thus, the greater cerebrovascular WML-burden observed in moderate-accumulators might be related to their older age[47] and to their poor outcomes in geriatric depression[48]. Furthermore, it is widely recognized that non-AD pathologies are highly prevalent in individuals with AD neuropathological changes and may interact with neurodegenerative processes in AD, leading to worsened outcomes[49]. Unfortunately, our study was limited by the exclusion of participants with vascular pathology etiologies and the lack of biomarkers to assess the presence of comorbid non-AD pathologies in living individuals with AD pathological changes. These limitations prevent us from drawing any definitive conclusions about the involvement of non-AD pathologies in the different tau accumulation profile groups. Therefore, it is essential for future studies to investigate the underlying pathological differences between these groups, including the potential contribution of non-AD pathologies.

We found that the rates of tau accumulation were particularly significant in Braak III–IV regions for the moderate-accumulators and further expanded to Braak V-VI regions for the fast-accumulators, consistent with neuropathology reports[50]. Overall, moderate-accumulators and fast-accumulators showed increased tau deposition rates in a topographical manner, reflecting initial spreading of tau in early-stage AD, and accurately reproducing the topography reported in numerous independent cohorts[51]. This is consistent with the suggested "prion-like" network explaining the stereotypical pattern of AD pathology spread[52, 53], and is suggestive of the fact that structural and functional connectivity, rather than spatial proximity, likely plays a major role in the spread of misfolded proteins across the brain[41, 54].

Trials on monoclonal antibodies directed against Aβ plaques have been prescreening participants for evidence of Aβ and only recently for tau pathology[5]. Researchers have also begun developing tau-targeted vaccines[55]. The primary target of Aβ-lowering therapies may be patients with limited widespread tau, as baseline tau-PET can inform trajectories of accumulation and suggest optimal intervention for the greatest effectiveness of the treatment. From a clinical trial perspective, it is important to note that delivering interventions in temporal proximity to time-points of rapid AD protein burden acceleration, particularly in individuals with an aggressive trajectory of AD protein accumulation, can improve the efficiency and effectiveness of the trial. Moreover, while Aβ-PET is useful for detecting early-AD pathology, repeated tau-PET is a better indicator of disease progression. Studies have shown that tau-PET progression is associated with future cognitive decline across the AD clinical spectrum[16, 56]. In CUs, tau accumulation rate in the inferior temporal neocortex, which aligns with the progression from preclinical AD to MCI, was associated with the cognitive decline[11]. However, it's important to acknowledge that individual variations in tau accumulation rates and disease progression exist. Therefore, a more effective strategy for clinical trial recruitment could be to identify individuals with a targeted tau accumulation rate at baseline, such as moderate-to-fast, depending on their disease stage. In the present study, we effectively identified individuals on a fast tau accumulation trajectory with 95% PPV from a single imaging time-point using a multiclass classification modeling. Our multiclass approach provides a comprehensive understanding of tau progression and its association with disease risk factors and patient characteristics,

with the potential to inform the development of more effective treatments for AD. A binary classification model to differentiate fast-accumulators and the rest could be explored in future studies for the operationalization of tau progression profiling. In hypothetical clinical trial scenarios, re-stratifying Aβ-positive early-AD participants for greater risk of future tau accumulation, resulted in a reduction in the required sample size by up to 77%. This is consistent with previous work showing that a smaller sample size is required to detect a clinically meaningful change in cognitive endpoints with trial cohorts screened for biomarkers relevant to the underlying biology that is targeted by the treatment[57].

The present study has some limitations. The current study is based on a convenience cohort where the degree of true population representation is unknown. Most notably, only 12% of our study cohort was diagnosed with dementia and 31% were cognitively impaired, limiting modeling of tau progression in later stages of the disease. This is reflected in our finding as 57% of the study cohort had stable longitudinal tau profile, which is consistent with previous subtyping approaches reporting that over 60% of the ADNI tau-PET cohort had no significant tau deposition trajectories[13]. However, our study differs from previous tau-burden subtyping studies in that we model tau progression patterns jointly with spatial and temporal information from longitudinal data. This is in contrast to identifying distinct spatial/stereotypical tau-burden patterns using cross-sectional data and inferring a theoretical model of longitudinal tau spreading, as was done in previous studies. Although, direct comparison of the results is challenging, we acknowledge the complementary information gained from the existing cross-sectional studies. We optimized the classifier based on PPV, not NPV, to maximize the probability that included subjects would have moderate-to-fast tau accumulation, and thus minimizing the dilutive contribution of non-progressing individuals with stable longitudinal tau profiles. This strategy resulted in the exclusion of some fast-accumulators but maximized the fraction of included subjects with stable low tau levels. We chose linear modeling of flortaucipir accumulation profiles due to limited follow-up durations in currently available longitudinal flortaucipir PET cohorts. The set of candidate independent predictors considered in this study, for tau accumulation profiles may not be exhaustive, but was selected to mimic a modeling approach practical in clinical trial designs. We chose to use flortaucipir because it is the most extensively studied tau-PET tracer, with the largest accessible cohorts and longitudinal studies. Additionally, flortaucipir is the only FDA-approved tracer for tau-PET to date. Other tau-PET tracers, such as ^{18}F-MK-6240 and ^{18}F-PI-2620, have been shown to exhibit patterns that follow the AD Braak staging[58, 59]. Thus, we expect the proposed tau progression profiling to be applicable to studies that utilize one of these tau radioligand or a combination of more than one tracer, if appropriate harmonization is performed. However, the different binding properties and off-target binding characteristics of different tau-PET tracers could affect our modeling results. Further independent validation, using other tau-PET tracers, is necessary to confirm generalizability of the detected tau progression profiles. Finally, while our tau progression profiling was performed blinded to clinical diagnosis, we observed increased prevalence of MCI and dementia diagnosis in moderate-accumulators and fast-accumulators compared to the stables, consistent with the expected dynamics of the tau progression with the clinical disease progression[15]. The interpretation of the diagnostic characteristics of the identified tau progression groups should be taken in the context of study specific recruitment

and clinical assessment protocols, though. Our findings may be limited by each cohort's inclusion and exclusion criteria, which may not reflect the broader AD population. Future studies are warranted to test the generalizability of our clustering and prediction models to other AD cohorts and populations with different demographics and clinical characteristics.

CONCLUSION

The ability to detect tau progression with baseline imaging and clinical biomarkers could potentially have a large impact on screening high-risk individuals for accelerated pathology progression, identifying treatment response or subgroups of responders, and for identifying risk factors, by better defining the biology. Overall, this study might have significant implications for designing effective pharmaceutical trials, as well as in the clinical practice once a disease modifying treatment becomes available, by stratifying individuals based on their probability to undergo greater pathological changes, which are characteristic and predictive of their clinical disease progression trajectories. Future studies are warranted to further validate and test the proposed clustering and prediction models on diverse cohorts. In addition, partnering with ongoing AD clinical trials to assess the real-life performance of these models in participant stratification in clinical trials is a promising future direction.

Supplementary Material

Refer to Web version on PubMed Central for supplementary material.

ACKNOWLEDGEMENT

FUNDING SOURCES

References

[1]. 2020 Alzheimer's disease facts and figures. Alzheimer's & dementia : the journal of the Alzheimer's Association. 2020.

[2]. Stocchetti N, Paterno R, Citerio G, Beretta L, Colombo A. Traumatic brain injury in an aging population. J Neurotrauma. 2012;29:1119–25 [PubMed: 22220762]

[3]. Budd Haeberlein S, O'Gorman J, Chiao P, Bussière T, von Rosenstiel P, Tian Y, et al. Clinical Development of Aducanumab, an Anti-Aβ Human Monoclonal Antibody Being Investigated for the Treatment of Early Alzheimer's Disease. J Prev Alzheimers Dis. 2017;4:255–63 [PubMed: 29181491]

[4]. Honig LS, Vellas B, Woodward M, Boada M, Bullock R, Borrie M, et al. Trial of Solanezumab for Mild Dementia Due to Alzheimer's Disease. N Engl J Med. 2018;378:321–30 [PubMed: 29365294]

[5]. Mintun MA, Lo AC, Duggan Evans C, Wessels AM, Ardayfio PA, Andersen SW, et al. Donanemab in Early Alzheimer's Disease. N Engl J Med. 2021;384:1691–704. [PubMed: 33720637]

[6]. van Dyck CH, Swanson CJ, Aisen P, Bateman RJ, Chen C, Gee M, et al. Lecanemab in Early Alzheimer's Disease. N Engl J Med. 2022.

[7]. Karran E, De Strooper B. The amyloid hypothesis in Alzheimer disease: new insights from new therapeutics. Nat Rev Drug Discov. 2022;21:306–18. [PubMed: 35177833]

[8]. Biel D, Brendel M, Rubinski A, Buerger K, Janowitz D, Dichgans M, et al. Tau-PET and in vivo Braak-staging as prognostic markers of future cognitive decline in cognitively normal to demented individuals. Alzheimer's research & therapy. 2021;13:137.

[9]. Pontecorvo MJ, Devous MD, Kennedy I, Navitsky M, Lu M, Galante N, et al. A multicentre longitudinal study of flortaucipir (18F) in normal ageing, mild cognitive impairment and Alzheimer's disease dementia. Brain. 2019;142:1723–35. [PubMed: 31009046]

[10]. Lu M, Pontecorvo MJ, Devous MD Sr., Arora AK, Galante N, McGeehan A, et al. Aggregated Tau Measured by Visual Interpretation of Flortaucipir Positron Emission Tomography and the Associated Risk of Clinical Progression of Mild Cognitive Impairment and Alzheimer Disease: Results From 2 Phase III Clinical Trials. JAMA neurology. 2021;78:445–53. [PubMed: 33587110]

[11]. Hanseeuw BJ, Betensky RA, Jacobs HIL, Schultz AP, Sepulcre J, Becker JA, et al. Association of Amyloid and Tau With Cognition in Preclinical Alzheimer Disease: A Longitudinal Study. JAMA neurology. 2019;76:915–24. [PubMed: 31157827]

[12]. Melis RJF, Haaksma ML, Muniz-Terrera G. Understanding and predicting the longitudinal course of dementia. Curr Opin Psychiatry. 2019;32:123–9. [PubMed: 30557268]

[13]. Vogel JW, Young AL, Oxtoby NP, Smith R, Ossenkoppele R, Strandberg OT, et al. Four distinct trajectories of tau deposition identified in Alzheimer's disease. Nature medicine. 2021;27:871–81.

[14]. Sintini I, Martin PR, Graff-Radford J, Senjem ML, Schwarz CG, Machulda MM, et al. Longitudinal tau-PET uptake and atrophy in atypical Alzheimer's disease. NeuroImage Clinical. 2019;23:101823. [PubMed: 31004914]

[15]. Jack CR Jr., Wiste HJ, Schwarz CG, Lowe VJ, Senjem ML, Vemuri P, et al. Longitudinal tau PET in ageing and Alzheimer's disease. Brain. 2018;141:1517–28. [PubMed: 29538647]

[16]. Cho H, Choi JY, Lee HS, Lee JH, Ryu YH, Lee MS, et al. Progressive Tau Accumulation in Alzheimer Disease: 2-Year Follow-up Study. Journal of nuclear medicine : official publication, Society of Nuclear Medicine. 2019;60:1611–21. [PubMed: 30926651]

[17]. Giorgio J, Jagust WJ, Baker S, Landau SM, Tino P, Kourtzi Z, et al. A robust and interpretable machine learning approach using multimodal biological data to predict future pathological tau accumulation. Nature communications. 2022;13:1887.

[18]. Weiner MW, Veitch DP, Aisen PS, Beckett LA, Cairns NJ, Green RC, et al. The Alzheimer's Disease Neuroimaging Initiative 3: Continued innovation for clinical trial improvement. Alzheimer's & dementia : the journal of the Alzheimer's Association. 2017;13:561–71.

[19]. Dagley A, LaPoint M, Huijbers W, Hedden T, McLaren DG, Chatwal JP, et al. Harvard Aging Brain Study: Dataset and accessibility. Neuroimage. 2017;144:255–8. [PubMed: 25843019]

[20]. Landau S, Thomas B, Thurfjell L, Schmidt M, Margolin R, Mintun M, et al. Amyloid PET imaging in Alzheimer's disease: a comparison of three radiotracers. European journal of nuclear medicine and molecular imaging. 2014;41:1398–407. [PubMed: 24647577]

[21]. Sperling RA, Mormino EC, Schultz AP, Betensky RA, Papp KV, Amariglio RE, et al. The impact of amyloid-beta and tau on prospective cognitive decline in older individuals. Annals of neurology. 2019;85:181–93. [PubMed: 30549303]

[22]. Tosun D, Landau S, Aisen PS, Petersen RC, Mintun M, Jagust W, et al. Association between tau deposition and antecedent amyloid-beta accumulation rates in normal and early symptomatic individuals. Brain. 2017.

[23]. Johnson KA, Schultz A, Betensky RA, Becker JA, Sepulcre J, Rentz D, et al. Tau positron emission tomographic imaging in aging and early Alzheimer disease. Annals of neurology. 2016;79:110–9. [PubMed: 26505746]

[24]. Southekal S, Devous MD Sr., Kennedy I, Navitsky M, Lu M, Joshi AD, et al. Flortaucipir F 18 Quantitation Using Parametric Estimation of Reference Signal Intensity. Journal of nuclear medicine : official publication, Society of Nuclear Medicine. 2018;59:944–51. [PubMed: 29191858]

[25]. Young CB, Landau SM, Harrison TM, Poston KL, Mormino EC. Influence of common reference regions on regional tau patterns in cross-sectional and longitudinal [(18)F]-AV-1451 PET data. Neuroimage. 2021;243:118553. [PubMed: 34487825]

[26]. Meltzer CC, Leal JP, Mayberg HS, Wagner HN Jr., Frost JJ. Correction of PET data for partial volume effects in human cerebral cortex by MR imaging. J Comput Assist Tomogr. 1990;14:561–70. [PubMed: 2370355]

[27]. Avants BB, Tustison NJ, Wu J, Cook PA, Gee JC. An open source multivariate framework for n-tissue segmentation with evaluation on public data. Neuroinformatics. 2011;9:381–400. [PubMed: 21373993]

[28]. Desikan RS, Segonne F, Fischl B, Quinn BT, Dickerson BC, Blacker D, et al. An automated labeling system for subdividing the human cerebral cortex on MRI scans into gyral based regions of interest. Neuroimage. 2006;31:968–80. [PubMed: 16530430]

[29]. Schwarz AJ, Yu P, Miller BB, Shcherbinin S, Dickson J, Navitsky M, et al. Regional profiles of the candidate tau PET ligand 18F-AV-1451 recapitulate key features of Braak histopathological stages. Brain. 2016;139:1539–50. [PubMed: 26936940]

[30]. Braak H, Alafuzoff I, Arzberger T, Kretzschmar H, Del Tredici K. Staging of Alzheimer disease-associated neurofibrillary pathology using paraffin sections and immunocytochemistry. Acta neuropathologica. 2006;112:389–404. [PubMed: 16906426]

[31]. Wilcock GK, Esiri MM. Asymmetry of pathology in Alzheimer's disease. J Neurol Neurosurg Psychiatry. 1987;50:1384–6. [PubMed: 3681321]

[32]. Walker JM, Fudym Y, Farrell K, Iida MA, Bieniek KF, Seshadri S, et al. Asymmetry of Hippocampal Tau Pathology in Primary Age-Related Tauopathy and Alzheimer Disease. J Neuropathol Exp Neurol. 2021;80:436–45. [PubMed: 33860327]

[33]. Fahmi R A PET only 18F-flortaucipir quantification: comparison with an MRI-based method. European journal of nuclear medicine and molecular imaging. 2021;48:S172.

[34]. Jack CR Jr., Wiste HJ, Weigand SD, Therneau TM, Lowe VJ, Knopman DS, et al. Defining imaging biomarker cut points for brain aging and Alzheimer's disease. Alzheimer's & dementia : the journal of the Alzheimer's Association. 2017;13:205–16.

[35]. Cummings J, Lee G, Ritter A, Sabbagh M, Zhong K. Alzheimer's disease drug development pipeline: 2020. Alzheimer's & Dementia: Translational Research & Clinical Interventions. 2020;6:e12050. [PubMed: 32695874]

[36]. Ossenkoppele R, Rabinovici GD, Smith R, Cho H, Schöll M, Strandberg O, et al. Discriminative Accuracy of [18F]flortaucipir Positron Emission Tomography for Alzheimer Disease vs Other Neurodegenerative Disorders. Jama. 2018;320:1151–62. [PubMed: 30326496]

[37]. Iddi SaD Michael C. Power and Sample Size for Longitudinal Models in R – The longpower Package and Shiny App. The R Journal. 2022;14:264–82.

[38]. Harrison TM, La Joie R, Maass A, Baker SL, Swinnerton K, Fenton L, et al. Longitudinal tau accumulation and atrophy in aging and alzheimer disease. Annals of neurology. 2019;85:229–40. [PubMed: 30597624]

[39]. Crary JF, Trojanowski JQ, Schneider JA, Abisambra JF, Abner EL, Alafuzoff I, et al. Primary age-related tauopathy (PART): a common pathology associated with human aging. Acta neuropathologica. 2014;128:755–66. [PubMed: 25348064]

[40]. Lee WJ, Brown JA, Kim HR, La Joie R, Cho H, Lyoo CH, et al. Regional Aβ-tau interactions promote onset and acceleration of Alzheimer's disease tau spreading. Neuron. 2022.

[41]. Vogel JW, Iturria-Medina Y, Strandberg OT, Smith R, Levitis E, Evans AC, et al. Spread of pathological tau proteins through communicating neurons in human Alzheimer's disease. Nature communications. 2020;11:2612.

[42]. Soldan A, Pettigrew C, Fagan AM, Schindler SE, Moghekar A, Fowler C, et al. ATN profiles among cognitively normal individuals and longitudinal cognitive outcomes. 2019;92:e1567–e79.

[43]. Silbert L, Erten-Lyons D, Kaye J, Tran H, Stanfield S, Quinn J, et al. O3-09-01: Alzheimer's disease pathology burden associated with clinical dementia decreases with age. Alzheimer's & Dementia. 2012;8:P446-P.

[44]. Power MC, Mormino E, Soldan A, James BD, Yu L, Armstrong NM, et al. Combined neuropathological pathways account for age-related risk of dementia. Annals of neurology. 2018;84:10–22. [PubMed: 29944741]

[45]. Savva GM, Wharton SB, Ince PG, Forster G, Matthews FE, Brayne C, et al. Age, neuropathology, and dementia. N Engl J Med. 2009;360:2302–9. [PubMed: 19474427]

[46]. Nelson AR, Sweeney MD, Sagare AP, Zlokovic BV. Neurovascular dysfunction and neurodegeneration in dementia and Alzheimer's disease. Biochimica et biophysica acta. 2016;1862:887–900. [PubMed: 26705676]

[47]. Garnier-Crussard A, Bougacha S, Wirth M, André C, Delarue M, Landeau B, et al. White matter hyperintensities across the adult lifespan: relation to age, Aβ load, and cognition. Alzheimer's research & therapy. 2020;12:127.

[48]. Aizenstein HJ, Baskys A, Boldrini M, Butters MA, Diniz BS, Jaiswal MK, et al. Vascular depression consensus report - a critical update. BMC Med. 2016;14:161. [PubMed: 27806704]

[49]. Latimer CS, Liachko NF. Tau and TDP-43 synergy: a novel therapeutic target for sporadic late-onset Alzheimer's disease. GeroScience. 2021;43:1627–34. [PubMed: 34185246]

[50]. Braak H, Thal DR, Ghebremedhin E, Del Tredici K. Stages of the pathologic process in Alzheimer disease: age categories from 1 to 100 years. J Neuropathol Exp Neurol. 2011;70:960–9. [PubMed: 22002422]

[51]. Maass A, Landau S, Baker SL, Horng A, Lockhart SN, La Joie R, et al. Comparison of multiple tau-PET measures as biomarkers in aging and Alzheimer's disease. Neuroimage. 2017;157:448–63. [PubMed: 28587897]

[52]. Braak H, Del Tredici K. Spreading of Tau Pathology in Sporadic Alzheimer's Disease Along Cortico-cortical Top-Down Connections. Cereb Cortex. 2018;28:3372–84. [PubMed: 29982389]

[53]. Morales R, Estrada LD, Diaz-Espinoza R, Morales-Scheihing D, Jara MC, Castilla J, et al. Molecular cross talk between misfolded proteins in animal models of Alzheimer's and prion diseases. J Neurosci. 2010;30:4528–35. [PubMed: 20357103]

[54]. Franzmeier N, Dewenter A, Frontzkowski L, Dichgans M, Rubinski A, Neitzel J, et al. Patient-centered connectivity-based prediction of tau pathology spread in Alzheimer's disease. Sci Adv. 2020;6.

[55]. Novak P, Kovacech B, Katina S, Schmidt R, Scheltens P, Kontsekova E, et al. ADAMANT: a placebo-controlled randomized phase 2 study of AADvac1, an active immunotherapy against pathological tau in Alzheimer's disease. Nature Aging. 2021;1:521–34. [PubMed: 37117834]

[56]. Jack CR, Wiste HJ, Weigand SD, Therneau TM, Lowe VJ, Knopman DS, et al. Predicting future rates of tau accumulation on PET. Brain. 2020;143:3136–50. [PubMed: 33094327]

[57]. Insel PS, Mattsson N, Mackin RS, Kornak J, Nosheny R, Tosun-Turgut D, et al. Biomarkers and cognitive endpoints to optimize trials in Alzheimer's disease. Annals of clinical and translational neurology. 2015;2:534–47. [PubMed: 26000325]

[58]. Pascoal TA, Benedet AL, Tudorascu DL, Therriault J, Mathotaarachchi S, Savard M, et al. Longitudinal 18F-MK-6240 tau tangles accumulation follows Braak stages. Brain. 2021;144:3517–28. [PubMed: 34515754]

[59]. Rullmann M, Brendel M, Schroeter ML, Saur D, Levin J, Perneczky RG, et al. Multicenter (18)F-PI-2620 PET for In Vivo Braak Staging of Tau Pathology in Alzheimer's Disease. Biomolecules. 2022;12.

RESEARCH IN CONTEXT

Systematic review:

The authors reviewed PubMed, Google Scholar, and reference lists of relevant research articles. Some studies have shown heterogeneity in tau accumulation and spread patterns in Alzheimer's disease (AD) which may contribute to variability in the disease course and individual response to treatments targeting AD pathology. However, the magnitude of accumulation rates is usually based on change at the last available measurements reflecting current patient status without accounting for potential heterogeneity in dynamics of temporal profiles and spatial patterns.

Interpretation:

Our modeling approach identified three distinct spatiotemporal patterns of tau progression, which are predictable from baseline tau-PET and clinical data with 81%-95% PPV. Screening for Aβ-positivity and fast tau accumulation could deliver up to 77% reduction in required sample size in clinical trials of Aβ-targeting drugs.

Future Directions:

Future work should further validate tau biomarker enrichment for designing effective pharmaceutical trials by stratifying high-risk individuals for accelerated pathology progression and assessing whether such enrichment criteria introduce biases to trial outcomes.
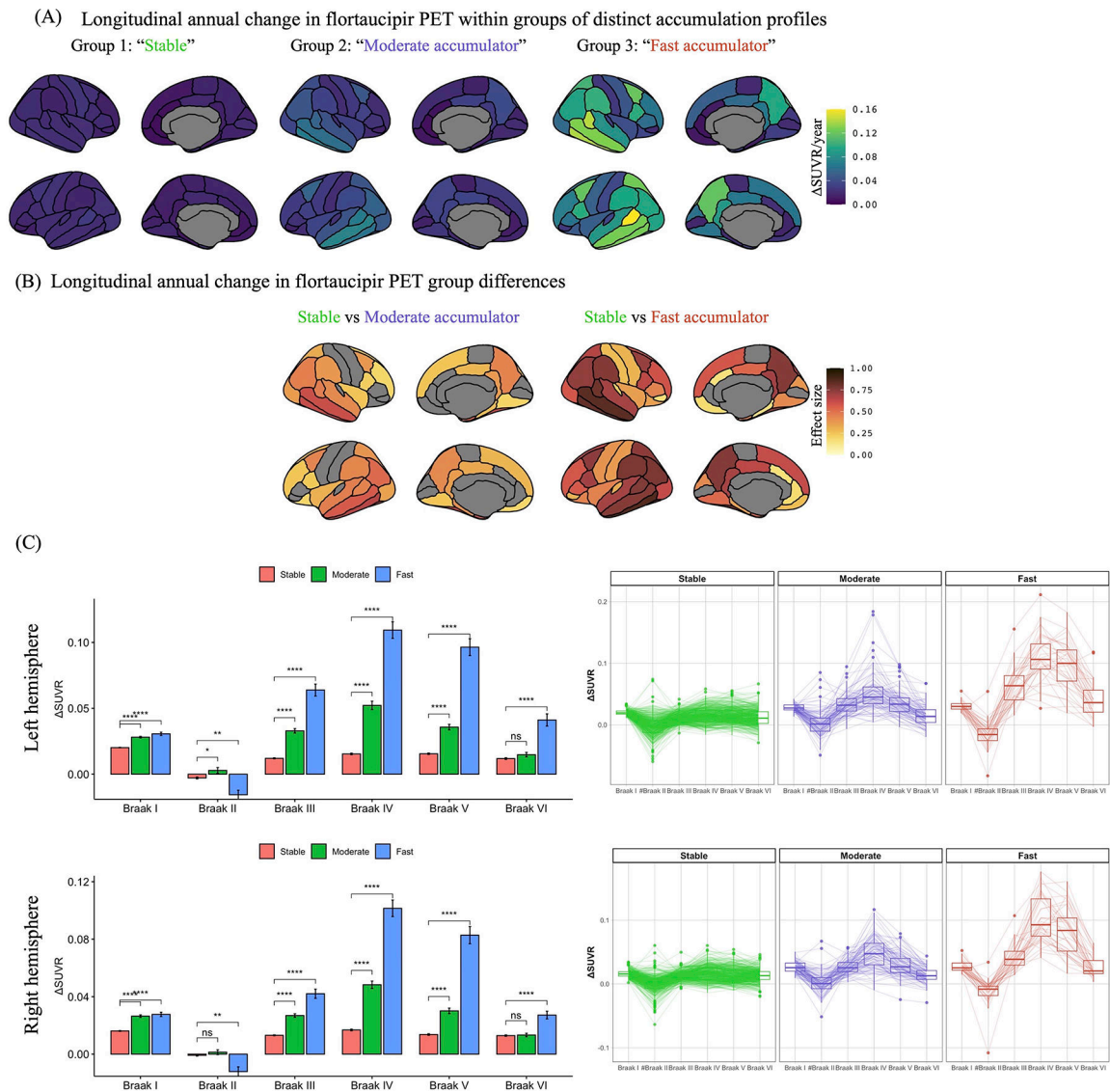
Figure 1.
Longitudinal flortaucipir progression rates for three distinct accumulation groups in the ADNI, AVID-05, and HABS cohorts. Plots represent annual change in flortaucipir positron emission tomography (PET) standard uptake value ratios (SUVRs) within each group (A) and estimated effect sizes (FDR adjusted p<0.01) between accumulators and their stable counterparts in anatomical regions-of-interest (B). (C) Bar and box plots represent the annual change and variance in left and right Braak I – VI SUVRs within each group, respectively. # Braak II region was not included in the clustering model. * and *** represent statistically significant group differences compared to the stable group at p<0.05 and p<10^{-16}, respectively.
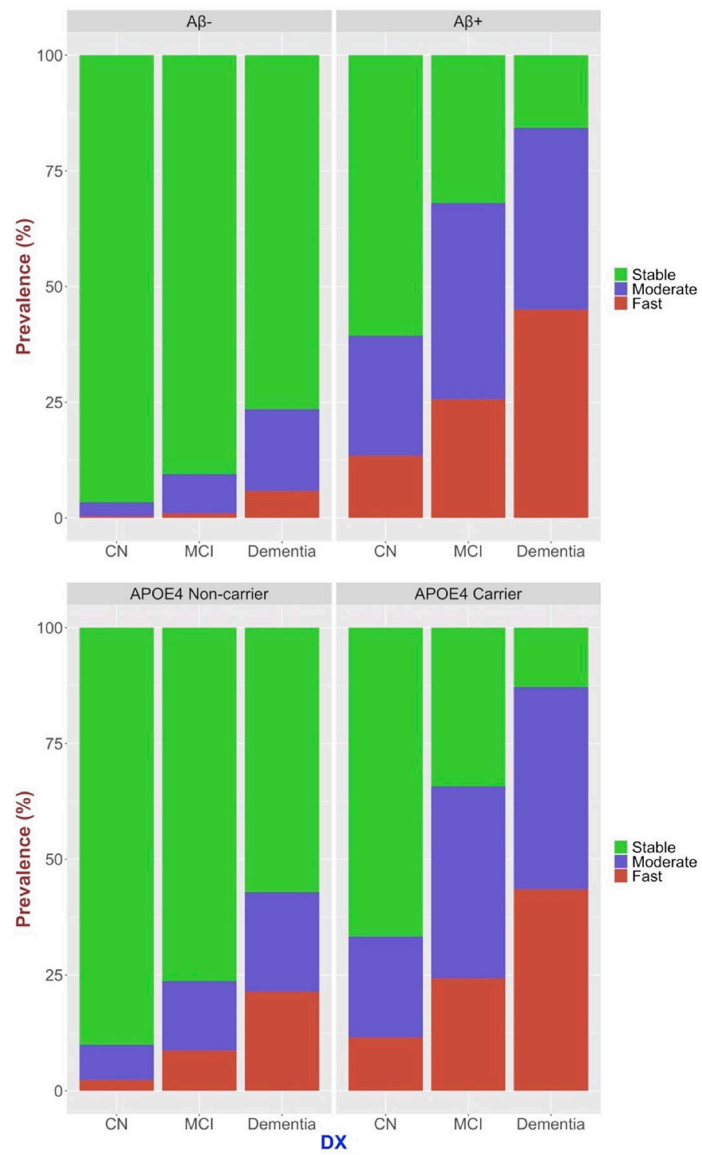
Figure 2.
Distribution of stable, moderate accumulator, and fast accumulator flortaucipir-progression profiles with respect to Aβ-positivity, cognitive impairment, and APOE-ε4 carrier status.

(A) Baseline flortaucipir SUVR group differences

(B) Baseline flortaucipir SUVR in regions of Braak stages I-VI
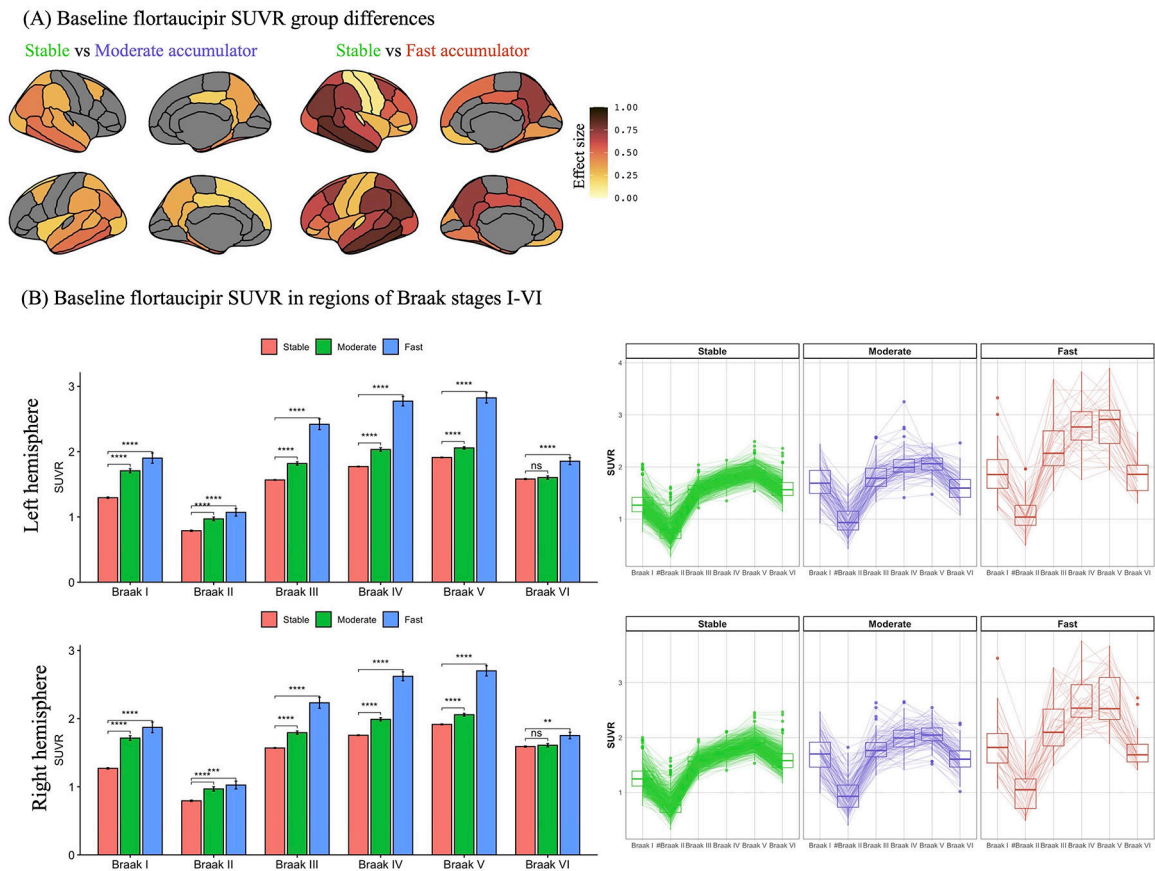
Figure 3.

Baseline characteristics of the three distinct flortaucipir progression groups in the ADNI, AVID-05, and HABS cohorts. Plots represent estimated baseline flortaucipir positron emission tomography (PET) standard uptake value ratios (SUVRs) effect sizes (FDR adjusted p<0.01) between accumulators and their stable counterparts in anatomical regions-of-interest (A). (B) The radar and box plots represent baseline flortaucipir PET Braak SUVRs within each group. #Braak II region was not included in the clustering model. * and *** represent statistically significant group differences compared to the stable group at p<0.05 and p<10^{-16}, respectively.
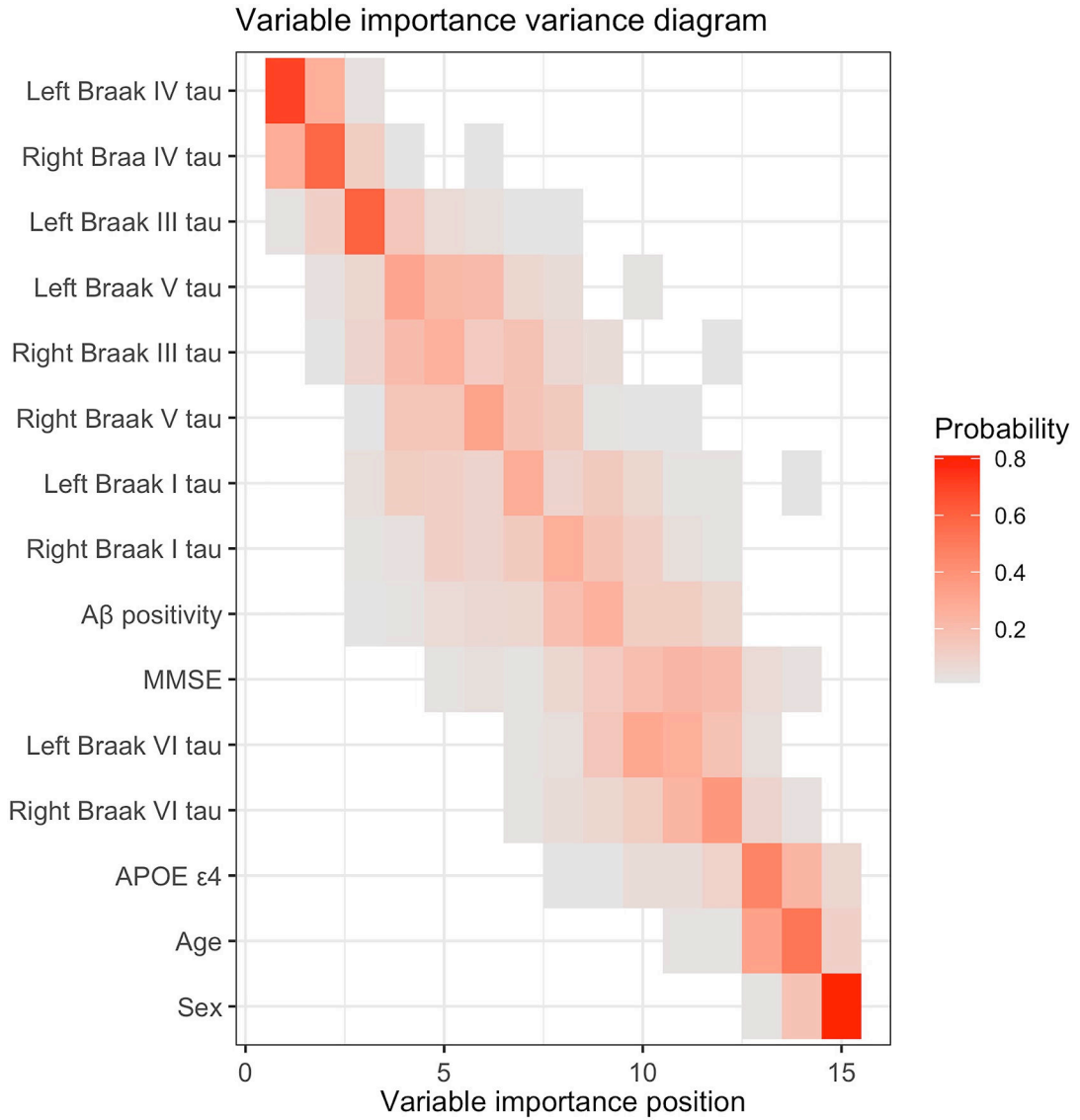
Figure 4.
Variable importance variance diagram for the multiclass random forest classifier to predict the longitudinal flortaucipir progression groups: stable, moderate accumulator, and fast accumulator. Each entry represents the probability of the baseline variable of interest (position on the y-axis) ranking at variable importance position on the x-axis, ranging from 0 in white to 1 in red. The positional variance diagram shows the variability of variable importance as measured by the multiclass random forest model from each cross-validation iteration. Each row represents a candidate predictor variable included in the multiclass random forest modeling, while each column represents a position in variable importance. The color of each entry corresponds to the probability of occurrences of that predictor variable at that variable importance position. The rows are ordered to rank predictor variables based on their average variable importance position across all cross-validation iterations. For example, the tau burden from bilateral Braak IV ROIs ranks in the top two

in the variable importance ordering in 60-70% of cross-validation iterations, while sex ranks the lowest in more than 80% of the cross-validation iterations.
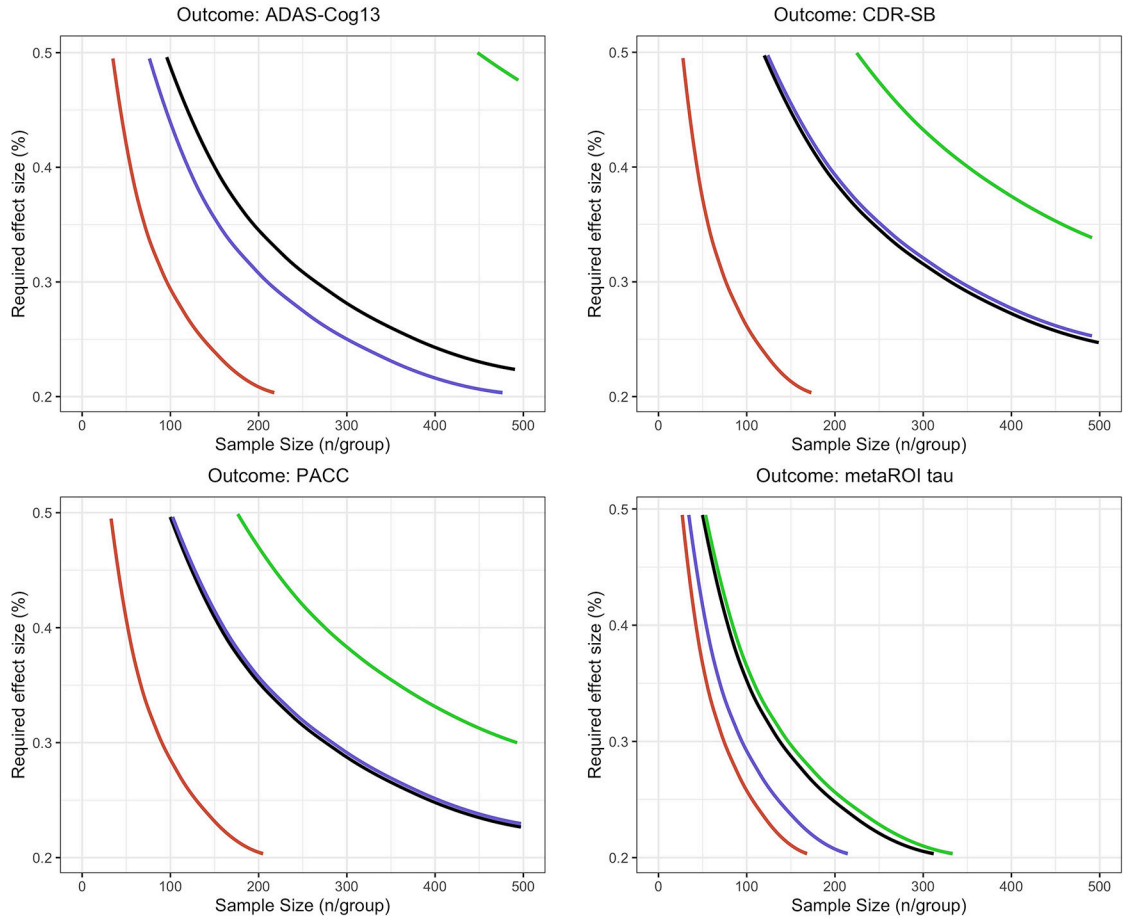
Figure 5.
Required Treatment Effect and Sample Size Calculations. Required treatment effect sizes are plotted against sample sizes in an 18-month trial for four enrichment schemes – black: screened for evidence of Aβ pathology but with variable tau progression; green: screened for evidence of Aβ pathology and stable tau profile; blue: screened for evidence of Aβ pathology and moderate tau accumulation profile; and red: screened for evidence of Aβ pathology and fast tau accumulation profile. The plotted curves show the combinations of the required treatment effect and sample size to achieve 80% power for clinical outcome measures of ADAS-Cog and CDR-SB and biomarker outcome measures of tau burden in the metaROI, Braak III, Braak IV, and Braak V regions.

Table 1:

Demographics, cognitive scores, AD biomarker characteristic, and number of flortaucipir PET scans within study cohorts. Baseline refers to first flortaucipir PET observation time point.

Variables	ADNI (N=326)		AVID-05 (N=161)		HABS (N=126)	
	Mean (SD)	Range	Mean (SD)	Range	Mean (SD)	Range
Age (years; baseline)	74.2 (7.3)	[55.7,92.2]	71.0 (9.7)	[50.0,95.0]	75.7 (6.1)	[64.8,90.0]
Education	16.4 (2.7)	[8,20]	15.5 (2.2)	[8,18]	16.0 (3.1)	[8,20]
Duration of flortaucipir PET follow-up (years)	2.2 (1.1)	[0.65,5.9]	1.4 (0.3)	[0.6, 1.9]	2.4 (0.9)	[1.2,5.6]
% Female (N)	48% (157)		49% (79)		56% (70)	
% Black or African American (N)	5.6% (18)		N/A		13.6% (17)	
% Asian (N)	0.9% (3)		N/A		0.8% (1)	
% Hispanic or Latinx (N)	5.6% (18)		N/A		0% (0)	
% CU (N) (baseline)	52% (171)		32% (51)		100% (126)	
% MCI (N) (baseline)	34% (111)		48% (77)		0% (0)	
% Dementia (N) (baseline)	13% (44)		20% (33)		0% (0)	
% w/ 2-timepoint flortaucipir PET scans	56% (184)		20% (32)		86% (108)	
% w/ 3-timepoint flortaucipir PET scans	44% (142)		80% (129)		14% (18)	

APOE: apolipoprotein E gene; MMSE: Mini-Mental State Examination; PET: positron emission tomography

Table 2.

Demographics, cognitive scores, Alzheimer's disease biomarker and risk characteristics for the three flortaucipir progression groups in ADNI, AVID-05, and HABS cohorts. Baseline refers to first flortaucipir PET observation time point.

	Stable (N=440)	Moderate accumulator (N=96)	Fast accumulator (N=38)	Stable vs Moderate accumulator	Stable vs Fast accumulator	Moderate accumulator vs Fast accumulator	Uncertain classification[*] (N=39)
Variables	Mean (SD)	Mean (SD)	Mean (SD)	Pr	Pr	Pr	Mean (SD)
Age (years; baseline)	73.1 (7.7)	76.1 (7.3)	70.6 (9.8)	**<0.001**	**0.05**	**<0.001**	76.7 (8.0)
Education	16.2 (2.8)	16.3 (2.3)	15.1 (2.3)	0.55	**0.02**	**0.005**	16.0 (2.5)
MMSE (baseline)	28.7 (1.8)	26.5 (3.3)	23.0 (4.2)	**<0.001**	**<0.001**	**<0.001**	26.8 (2.6)
MMSE[##]	−0.04 (0.33)	−0.6 (0.7)	−1.7 (0.9)	**<0.001**	**<0.001**	**<0.001**	−0.57 (0.55)
CDR-SB[#] (baseline)	0.46 (1.1)	1.5 (1.6)	4.4 (3.0)	**<0.001**	**<0.001**	**<0.001**	1.7 (2.0)
CDR-SB[##]	0.09 (0.3)	0.5 (0.6)	1.5 (0.8)	**<0.001**	**<0.001**	**<0.001**	0.45 (0.46)
ADAS-Cog[#] (baseline)	9.3 (4.2)	13.6 (6.2)	21.4 (6.9)	**<0.001**	**<0.001**	**<0.001**	14.2 (5.2)
ADAS-Cog[##]	1.1 (0.4)	1.6 (0.6)	2.7 (0.7)	**<0.001**	**<0.001**	**<0.001**	1.6 (0.50)
GDS[#] (baseline)	1.9 (2.6)	2.1 (2.1)	1.8 (1.8)	0.59	0.83	0.56	1.8 (2.3)
GDS[##]	0.06 (0.15)	0.12 (0.14)	0.10 (0.17)	**0.04**	0.37	0.72	0.084 (0.16)
WML [##] burden (cc; baseline)	1.2 (8.0)	5.8 (17.8)	3.8 (8.2)	**0.01**	0.09	0.91	3.07 (10.7)
Meta ROI thickness (mm; baseline)	3.0 (0.32)	2.6 (0.40)	2.5 (0.45)	**<0.001**	**<0.001**	0.29	2.7 (0.40)
Duration of flortaucipir PET follow-up (years)	2.2 (1.1)	1.7 (0.8)	1.5 (0.5)	**<0.001**	**<0.001**	0.17	1.7 (0.9)
% Female (N)	50% (218)	55% (53)	55% (21)	0.37	0.61	1	36% (14)
% Black or African American[#] (N)	7.7% (26/338)	6.2% (4/64)	0% (0/18)				18% (5/27)
% Asian[#] (N)	0.6% (2/338)	0% (0/64)	0% (0/18)				7% (2/27)
% Hispanic or Latinx[#] (N)	3.5% (12/339)	4.7% (3/64)	5.6% (1/18)	0.72	0.50	1.0	26% (7/27)
% APOE ε4 carriers (N)	30% (131)	63% (61)	71% (27)	**<0.001**	**0.002**	0.88	63% (22/35)
% Aβ(N) (first observation)	32% (141)	88% (84)	97% (37)	**<0.001**	**<0.001**	0.18	69% (27)
% CU (N) (first observation)	70% (308)	29% (28)	0% (0)	**<0.001**	**<0.001**	**<0.001**	31% (12)
% MCI (N) (first observation)	25% (111)	47% (45)	37% (14)				46% (18)
% Dementia (N) (first observation)	5% (21)	24% (23)	63% (24)				23% (9)
% w/ 2-timepoint flortaucipir PET scans (N)	54% (240)	52% (50)	39% (15)	0.73	0.09	0.25	49% (19)
% w/ 3-timepoint flortaucipir PET scans (N)	46% (200)	48% (46)	61% (23)				51% (20)
% ADNI cases (N)	52% (228)	60% (58)	47% (18)	**<0.001**	**<0.001**	**0.04**	56% (22)

Variables	Stable (N=440) Mean (SD)	Moderate accumulator (N=96) Mean (SD)	Fast accumulator (N=38) Mean (SD)	Stable *vs* Moderate accumulator Pr	Stable *vs* Fast accumulator Pr	Moderate accumulator *vs* Fast accumulator Pr	Uncertain classification[*] (N=39) Mean (SD)
% AVID-05 cases (N)	22% (98)	32% (31)	53% (20)				31% (5)
% HABS cases (N)	26% (114)	7% (7)	0% (0)				23% (5)

APOE: apolipoprotein E gene; cc: cubic centimeter; CDR-SB: Clinical Dementia Rating – Sum of Boxes; GDS: Geriatric Depression Score; MMSE: Mini-Mental State Examination; PET: positron emission tomography

[#] Data only available for ADNI and HABS participants.

[##] Data only available for ADNI participants.

[*] Uncertain classification based on highest posterior density credible intervals; 46% (18/39) were classified as stable, 41% (16/39) as moderate progressor, and 13% (5/39) as fast progressor

Table 3.

Scenarios of biomarker-based enrichment in placebo-controlled trial for clinical populations with evidence of AD pathology based on Aβ PET imaging. The sample size required to detect a 30% slowing in change in outcome measures with 80% power, along with the estimated annual rates of change in outcome measures, are reported as mean [95% CI].

			ADAS-13		CDR-SB		PACC		metaROI tau	
Population	Duration (months)	Enrichment	Annual rate of change	Sample size (n/group)	Annual rate of change	Sample size (n/group)	Annual rate of change	Sample size (n/group)	Annual rate of change	Sample size (n/group)
Early AD	18	Aβ+	3.07 [2.28,3.85]	266 [169,482]	1.03 [0.73,1.32]	333 [202,649]	−1.98 [−2.48,−1.47]	277 [176,499]	0.08 [0.06,0.1]	139 [92,233]
		Aβ+; moderate accumulator	2.67 [1.8,3.54]	212 [120,466]	0.85 [0.51,1.19]	344 [174,969]	−1.68 [−2.29,−1.06]	285 [152,711]	0.11 [0.08,0.14]	95 [60,173]
		Aβ+; fast accumulator	7 [4.47,9.53]	97 [52,238]	2.53 [1.76,3.29]	77 [45,158]	−4.14 [−5.58,−2.69]	91 [50,215]	0.07 [0.04,0.1]	75 [38,208]
AD	18	Aβ+	4.52 [3.14,5.91]	198 [116,412]	1.92 [1.49,2.34]	119 [80,197]	−3.1 [−4.05,−2.15]	220 [129,458]	0.09 [0.06,0.12]	172 [98,382]
		Aβ+; moderate accumulator	2.29 [0.81,3.76]	337 [125,2657]	1.62 [0.89,2.36]	223 [106,748]	−2.14 [−3.37,−0.9]	293 [118,1634]	0.11 [0.06,0.15]	124 [59,421]
		Aβ+; fast accumulator	7.6 [5.06,10.14]	96 [54,217]	2.55 [1.95,3.15]	58 [38,100]	−4.65 [−6.34,−2.96]	129 [69,318]	0.09 [0.04,0.15]	225 [91,1204]
MCI	18	Aβ+	1.93 [1.26,2.61]	481 [264,1136]	0.41 [0.24,0.59]	694 [342,2102]	−1.2 [−1.6,−0.8]	463 [261,1034]	0.08 [0.06,0.1]	163 [103,298]
		Aβ+; moderate accumulator	2.71 [1.74,3.68]	227 [123,551]	0.5 [0.24,0.75]	443 [194,1877]	−1.32 [−1.92,−0.72]	383 [181,1286]	0.11 [0.09,0.14]	85 [54,154]
		Aβ+; fast accumulator	5.55 [3.47,7.62]	39 [20,98]	1.41 [0.19,2.64]	230 [66,1330]	−3.81 [−5.66,−1.95]	65 [29,245]	0.07 [0.03,0.11]	60 [26,257]
CU	48	Aβ+	0.54 [0.32,0.76]	496 [253,1375]	0.07 [0.03,0.11]	1267 [524,6382]	−0.29 [−0.44,−0.15]	663 [301,2484]	0.04 [0.02,0.05]	284 [166,596]
		Aβ+; moderate accumulator	1.32 [0.76,1.89]	96 [47,295]	0.35 [0.17,0.53]	187 [81,814]	−1.07 [−1.58,−0.55]	148 [68,547]	0.11 [0.07,0.14]	44 [25,97]